Electron Transfer on the Infrared Vibrational Time Scale in the Mixed Valence State of 1,4-Pyrazine- and 4,4‘-Bipyridine-Bridged Ruthenium Cluster Complexes

ARTICLE *in* JOURNAL OF THE AMERICAN CHEMICAL SOCIETY · APRIL 1999

Impact Factor: 12.11 · DOI: 10.1021/ja984000z

9 AUTHORS, INCLUDING:

Clifford P. Kubiak
University of California, San Diego
247 PUBLICATIONS **8,476** CITATIONS

SEE PROFILE

Electron Transfer on the Infrared Vibrational Time Scale in the Mixed Valence State of 1,4-Pyrazine- and 4,4′-Bipyridine-Bridged Ruthenium Cluster Complexes

Tasuku Ito,*,† Tomohiko Hamaguchi,† Haruko Nagino,† Tadashi Yamaguchi,† Hiroaki Kido,‡ Igor S. Zavarine,§ Todd Richmond,§ John Washington,§ and Clifford P. Kubiak*,§,⊥

Contribution from the Department of Chemistry, Tohoku University, Aoba, Aramaki, Aoba-ku, Sendai 980-8578, Japan, and Department of Chemistry, Purdue University, West Lafayette, Indiana 47907-1393

Received November 19, 1998

Abstract: Intramolecular electron transfers within the mixed valence states of the ligand bridged hexaruthenium clusters $Ru_3(\mu_3\text{-}O)(\mu\text{-}CH_3CO_2)_6(CO)(L)(\mu\text{-}L')Ru_3(\mu_3\text{-}O)(\mu\text{-}CH_3CO_2)_6(CO)(L)$ (L′ = 1,4-pyrazine; L = 4-dimethylaminopyridine (**1**), pyridine (**2**), 4-cyanopyridine (**3**), or L′ = 4,4′-bipyridine; L = 4-dimethylaminopyridine (**4**), pyridine (**5**), 4-cyanopyridine (**6**)) were examined. Two discrete and reversible single electron reductions are evident by cyclic voltammetry in the redox chemistry of **1**−**5**, and the intercluster charge-transfer complexes are well-defined. The splitting of the reduction waves, ΔE, is related to the electronic coupling H_{AB} between the triruthenium clusters, and varies from 80 mV for **5** to 440 mV for **1**. In the case of **6**, the splitting of the reduction waves, ΔE, is <50 mV and the intercluster charge-transfer complex is not defined. The mixed valence states of **1**−**3** also exhibit intervalence charge transfer (ICT) bands in the region 12 100 (**1**) to 10 800 cm^{-1} (**3**) which provide spectroscopic estimates of H_{AB} in the range 2180 (**1**) to 1310 cm^{-1} (**3**). The magnitude of the electronic coupling H_{AB} is found to strongly influence the IR spectra of the singly reduced (−1) mixed valence states of **1**−**6** in the ν(CO) region. In the case of relatively weak electronic coupling (**4**−**6**), two ν(CO) bands are clearly resolved. In the cases of strong electronic coupling (**1**−**3**), these bands broaden to a single ν(CO) absorption band. These data allow the rate constants, k_e, for electron transfer in the mixed valence states of **1**, **2**, and **3** to be estimated by simulating dynamical effects (Bloch-type equations) on ν(CO) absorption band shape at 9×10^{11}, 5×10^{11}, and ca. 1×10^{11} s^{-1}, respectively. The less strongly coupled 4,4′-bipyridine-bridged complexes **4**−**6** exhibit IR line shapes in the −1 mixed valence states that are not as strongly affected by electron-transfer dynamics. The rate constant for the −1 mixed valence state of **4** is close to the lower limit that can be estimated by this approach, between 1×10^{10} and 1×10^{11} s^{-1}.

Introduction

The question of whether a chemical system is fluctuating or static can only be answered with respect to the intrinsic time scale of observation. In NMR spectroscopy, the time scale of a "fluxional" process that will coalesce distinct static spectral features into an average spectrum is on the order of milliseconds. In IR spectroscopy, the time scale required is on the order of picoseconds, and convincing cases have been made that a chemical reaction in fluid solution could not be sufficiently fast to cause coalescence and averaging of an IR spectrum.[1] This is certainly true for a diffusion-controlled intermolecular process, but intramolecular processes, especially electron and energy transfer, can occur on the picosecond time scale or faster.[2] The semiclassical expression for the rate constant for intramolecular electron transfer, k_e, in a symmetric charge-transfer complex with no net free energy change ($\Delta G^0 = 0$) is given by eq 1

$$k_e = \kappa \nu_n \exp[-(\Delta G_\lambda^* - H_{AB} + H_{AB}^2/4\Delta G_\lambda^*)/RT] \quad (1)$$

where κ is the adiabaticity factor (unity for adiabatic reactions), ν_n is the nuclear frequency factor, which includes both the solvent dielectric response frequency and bond length/bond angle reorganizations required by charge transfer between the localized valence states, ΔG_λ^* is the reorganizational energy barrier, and H_{AB} is the electronic coupling between the exchanging centers.[3] The theoretical maximum rate constant for an intramolecular electron transfer thus can approach the nuclear frequency factor, ν_n (10^{12}−10^{13} s^{-1}) for barrierless ($H_{AB} = 2\Delta G_\lambda^*$) electron transfer. Here we describe our studies of 1,4-pyrazine- (hereafter abbreviated as pz) and 4,4′-bipyridine (bpy)-bridged dimers of trinuclear ruthenium clusters, $Ru_3(\mu_3\text{-}O)(\mu\text{-}CH_3CO_2)_6(CO)(L)(\mu\text{-}L')Ru_3(\mu_3\text{-}O)(\mu\text{-}CH_3CO_2)_6(CO)(L)$ (L′ = pz and L = 4-dimethylaminopyridine (dmap) (**1**), pyridine (py) (**2**), 4-cyanopyridine (cpy) (**3**); or L′ = (bpy) and L = dmap (**4**), py (**5**), cpy (**6**)). These complexes form reasonably stable charge-transfer complexes, with overall −1 charge, which

* To whom correspondence should be addressed.
† Tohoku University.
‡ Present address: College of Engineering, Nihon University, Koriyama 963-8642, Japan.
§ Purdue University.
⊥ Present address: Department of Chemistry and Biochemistry, University of California, San Diego, La Jolla, CA 92093-0358.

(1) Wood, K. A.; Strauss, H. L. *J. Phys. Chem.* **1990**, *94*, 5677.
(2) Hsiao, J.-S.; Krueger, B. P.; Wagner, R. W.; Johnson, T. E.; Delaney, J. K.; Mauzerall, D. C.; Fleming, G. R.; Lindsey, J. S.; Bocian, D. F.; Donohoe, R. J. *J. Am. Chem. Soc.* **1996**, *118*, 11181.
(3) Sutin, N. S. *Prog. Inorg. Chem.* **1983**, *30*, 441.

10.1021/ja984000z CCC: $18.00
Published on Web 04/29/1999

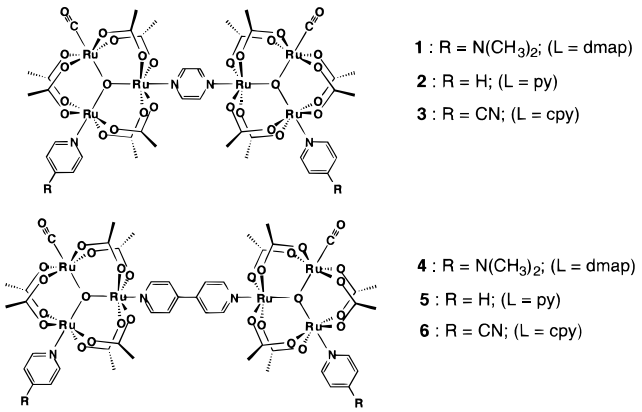

undergo rapid intramolecular electron transfer between the coupled Ru_3 clusters. In the most rapidly exchanging systems, spectral coalescence was observed in the ν(CO) infrared vibrational spectra. We now describe in detail the unusual characteristics of the IR spectra of the intervalence charge-transfer (ICT) states of complexes **1**−**3** that were communicated in part earlier,[4] and new studies on the related bpy-bridged complexes, **4**−**6**.

Results and Discussion

Synthesis of $Ru_3(\mu_3\text{-}O)(CH_3CO_2)_6(CO)(L)(\mu\text{-}L')Ru_3(\mu_3\text{-}O)(\mu\text{-}CH_3CO_2)_6(CO)(L)$ (1−6). The complexes **1**−**6**, which have one carbonyl and one pyridyl ligand per Ru_3 unit, were prepared by a labile ligand complex (the solvent complex $Ru_3(\mu_3\text{-}O)(CH_3CO_2)_6(CO)(L)(H_2O)$) and "metal complex as ligand ($Ru_3(\mu_3\text{-}O)(CH_3CO_2)_6(CO)(L)(L')$ where L′ = pz or bpy)" combination synthetic strategy.[5] It is known for this type of Ru_3 complex that the solvent ligand is labile and readily replaced by pyridyl ligands.[6] All clusters **1**−**6** were prepared as analytically pure crystalline solids. Complex **1** has been characterized by X-ray crystallography.[7] In the neutral isolated state, each trinuclear Ru_3 unit formally contains one Ru(II) and two Ru(III) centers and the carbonyl ligand is coordinated to the formally divalent center.[8]

Cyclic Voltammetry. The cyclic voltammograms of **1**−**5** each show four reversible redox processes (Figures 1 and 2). These are characterized by the half-wave potentials for the different redox processes, $E_{1/2}$(ox/red). Apparent two-electron oxidation waves are observed at approximately $E_{1/2}(+2/0) = +0.50$ and $E_{1/2}(+4/+2) = +1.3$ V vs SSCE.[9] Here, the overall charges of the complexes are expressed in parentheses. Each of the complexes **1**−**5** displays two single-electron reduction waves that correspond formally to $Ru_3^{III,III,II}$-L′-$Ru_3^{III,III,II}$/$Ru_3^{III,III,II}$-L′-$Ru_3^{III,II,II}$ (0/−1) and then $Ru_3^{III,III,II}$-L′-$Ru_3^{III,II,II}$/$Ru_3^{III,II,II}$-L′-$Ru_3^{III,II,II}$ (−1/−2) (Figures 1 and 2). In the case of **6,** the splitting between the (0/−1) and (−1/−2) states is too small (ΔE < 50 mV) to resolve by cyclic or differential pulse voltammetry. One important contribution to the magnitude of the splitting between the single-electron (0/−1) and (−1/−2) reduction waves, ΔE, is the stabilization energy imparted to the −1 state by electron delocalization.[10,11] In the case of **1**, $\Delta E = 440$ mV, and this corresponds to a comproportionation constant, $K_c = \exp(\Delta EF/RT) = 2.7 \times 10^7$, for the compropor-

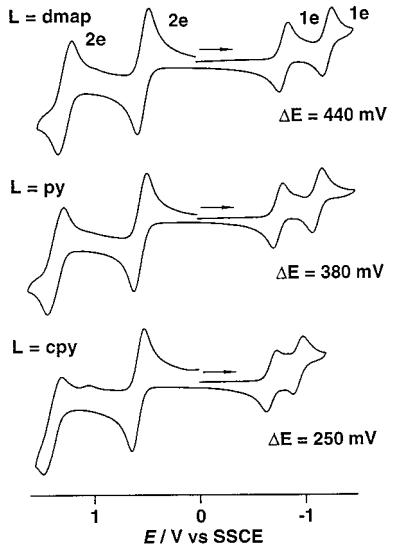

Figure 1. Cyclic voltammograms of **1** (top), **2** (middle), and **3** (bottom) with dichloromethane solvent, 0.1 M tetra-*n*-butylammonium hexaflurophosphate supporting electrolyte, and potentials referenced to the saturated sodium chloride calomel electrode (SSCE). ΔE is the difference between the half-wave potentials for the two one−electron reduction waves corresponding to the redox processes: $Ru_3^{III,III,II}$-pz-$Ru_3^{III,III,II}$/$Ru_3^{III,III,II}$-pz-$Ru_3^{III,II,II}$ (0/−1) and then $Ru_3^{III,III,II}$-pz-$Ru_3^{III,II,II}$/$Ru_3^{III,II,II}$-pz-$Ru_3^{III,II,II}$ (−1/−2).

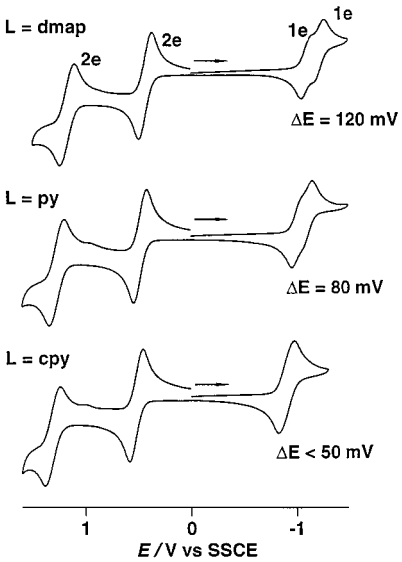

Figure 2. Cyclic voltammograms of **4** (top), **5** (middle) and **6** (bottom) with dichloromethane solvent, 0.1 M tetra-*n*-butylammonium hexafluro-phosphate supporting electrolyte, and potentials referenced to the saturated sodium chloride calomel electrode (SSCE). ΔE is the difference between the half-wave potentials for the two one-electron reduction waves corresponding to the redox processes: $Ru_3^{III,III,II}$-bpy-$Ru_3^{III,III,II}$/$Ru_3^{III,III,II}$-bpy-$Ru_3^{III,II,II}$ (0/−1) and then $Ru_3^{III,III,II}$-bpy-$Ru_3^{III,II,II}$/$Ru_3^{III,II,II}$-bpy-$Ru_3^{III,II,II}$ (−1/−2).

(4) Ito, T.; Hamaguchi, T.; Nagino, H.; Yamaguchi, T.; Washington, J.; Kubiak, C. P. *Science* **1997**, *277*, 660.

(5) Campagna, S.; Denti, G.; Serroni, S.; Ciano, M.; Balzani, V. *Inorg. Chem.* **1992**, *31*, 2982.

(6) Kido, H.; Nagino, H.; Ito, T. *Chem. Lett.* **1996**, 745.

(7) Crystal data for **1**·3$CHCl_3$: triclinic space group $P\bar{1}$, $a = 14.075(7)$ Å, $b = 16.450(5)$ Å, $c = 12.85(2)$ Å, $\alpha = 93.40(6)°$, $\beta = 112.23(6)°$, $\gamma = 88.09(3)°$, $V = 2748(4)$ Å^3, $Z = 1$. Details will be reported elsewhere.

(8) Abe, M.; Sasaki, Y.; Yamada. Y.; Tsukahara, K.; Yano, S.; Yamaguchi, T.; Tominaga, M.; Taniguchi, I.; Ito, T. *Inorg Chem.* **1996**, *35*, 6724.

(9) $E_{1/2}(+4/+2) = +1.24$ (**1**), +1.34 (**2**), +1.39 (**3**), +1.17 (**4**), +1.27 (**5**), +1.32 (**6**) V vs SSCE and $E_{1/2}(+2/0) = +0.50$ (**1**), +0.54 (**2**), +0.58 (**3**), +0.43 (**4**), +0.48 (**5**), +0.52 (**6**) V vs SSCE. In each series of pz- and bpy-bridged complexes, $E_{1/2}(+4/+2)$ and $E_{1/2}(+2/0)$ are systematically shifted toward positive potentials on going from electron-donating dmap in **1** (or **4**) to unsubstituted pyridine for **2** (or **5**) and then to electron-withdrawing cpy for **3** (or **6**).

(10) Richardson, D. E.; Taube, H. *Coord. Chem. Rev.* **1984**, *60*, 107.

(11) Richardson, D. E.; Taube, H. *Inorg. Chem.* **1981**, *20*, 1278.

Table 1. Electrochemical Data for $[Ru_3(\mu_3\text{-}O)(\mu\text{-}CH_3CO_2)_6(CO)(L)]_2(\mu\text{-}L')$ (L′ = pz, bpy) (**1**−**6**)

	L′	L	$E_{1/2}(0/-1)$,[a] V	$E_{1/2}(-1/-2)$,[a] V	ΔE (mV)	K_c
1	pz	dmap	−0.89	−1.33	440	2.7×10^7
2	pz	py	−0.81	−1.19	380	2.7×10^6
3	pz	cpy	−0.68	−0.93	250	1.7×10^4
4	bpy	dmap	−1.11	−1.23	120	1.1×10^2
5	bpy	py	−1.03	−1.11	80	2.3×10^1
6	bpy	cpy	−0.91	−0.91	<50	<10

[a] Cyclic voltammograms recorded in 0.1 M tetra-*n*-butylammonium hexafluorophosphate in dichloromethane, V, versus saturated sodium chloride calomel electrode (SSCE).

tionation equilibrium given in eq 2. It is useful to consider K_c as a stability constant reflecting the stabilization arising from electronic delocalization in the −1 state relative to the neutral and −2 states. The relationship between the electrochemical value of ΔE and the electronic coupling, H_{AB}, has been discussed.[10−14]

$$Ru_3^{III,III,II}\text{-}L'\text{-}Ru_3^{III,III,II} + Ru_3^{III,II,II}\text{-}L'\text{-}Ru_3^{III,II,II} \overset{K_c}{\rightleftharpoons} 2Ru_3^{III,III,II}\text{-}L'\text{-}Ru_3^{III,II,II} \quad (2)$$

An interesting aspect of these complexes is that the splitting, ΔE, between the (0/−1) and (−1/−2) states of **1**−**6** depends strongly on the ancillary ligands (dmap, py, cpy) and on the bridging ligands (pz, bpy). Thus, as the adjustable pyridyl ligand in the series **1**−**6** is changed from dmap in **1** and **4** to an unsubstituted pyridine for **2** and **5** to an electron-withdrawing cpy for **3** and **6**, the values of ΔE and K_c decrease considerably (Table 1). Indeed the comproportionation constants K_c fall by 7 orders of magnitude from **1** to **6**. To the extent that electrochemical ΔE values reflect the magnitude of the electronic coupling, H_{AB}, it is clear that H_{AB} can be moderated over a large range by a relatively simple ligand substitution. Remote ligand control of electronic coupling in mixed valence complexes is not unusual.[13−15] However, to our knowledge the wide variation seen in **1**−**6** has not been reported previously. In the present case, it appears that two conditions are simultaneously met: (i) very favorable overlap between the Ru_3 cluster dπ-electron system and the bridging pz or bpy π^* system, and (ii) the ability to raise or lower Ru_3 cluster d-electron levels engaging the pz or bpy π^* system by changing the electron donor/acceptor nature of the adjustable pyridyl ligand. The relevant Ru d level then is closer to the pz π^* level in **1** than it is in **3**, and closer to the bpy π^* level in **4** than it is in **6**. Three lines of experimental evidence support this description of the electronic structure: (i) the metal-to-ligand charge transfer (MLCT) electronic absorption bands for the Ru-d to pz π^* transition appear at increasing energies in the series **1**−**3** (482 nm in **1**, 475 nm (overlapped) in **2**, and 450 nm (overlapped) in **3**); (ii) the average of the reduction potentials $E_{1/2}(0/-1)$ and $E_{1/2}(-1/-2)$ becomes more positive in the series from **1** to **3** and from **4** to **6** (Table 1); and (iii) the same type of Ru_3 dimers (L = dmap, py, cpy) bridged by 1,4-diazabicyclo[2.2.2]octane (Dabco), which has no π-electron system, show no electronic coupling ($\Delta E \approx 0$).[16]

Although the trend in cyclic voltammetry data for compounds **4**−**6** with bpy as the bridging ligand is similar to that for compounds **1**−**3** (Table 1), the ΔE values for **4**−**6** are approximately 25% of the values for the pz-bridged complexes, **1**−**3**. In general, electronic coupling falls off exponentially with increasing distance between electronically interacting centers. The center-to-center separation between Ru_3O units in the crystal structure of **1** is 10.9 Å, and it is estimated at ca. 15.3 Å in **4**−**6**. The longer separation between Ru_3 centers in **4**−**6** (and possible nonplanarity of the bpy rings) decreases the intercluster electronic coupling, thereby decreasing ΔE values. The bridging ligand π-electron systems mediate electronic coupling between the two Ru_3 centers.

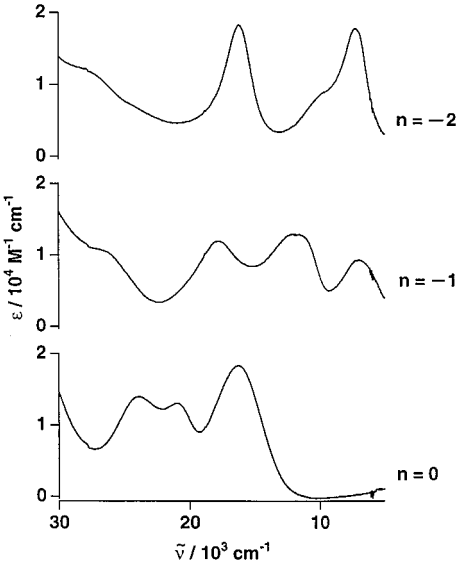

Figure 3. Electronic absorption spectal data for **1** in the neutral isolated ($n = 0$, bottom), 1-electron reduced ($n = -1$, middle), and 2-electron reduced ($n = -2$, top) states with 0.1 M tetra-*n*-butylammonium hexaflurophosphate dichloromethane solution at −10 °C.

Intervalence Charge Transfer in 1−**3.** To assess further the extent of electronic interaction between the two coupled Ru_3 units in the −1 states, intervalence charge transfer (ICT) spectra were examined. Figure 3 shows the electronic absorption spectra of the neutral, −1, and −2 states of **1**. The neutral species exhibits no absorptions in the near-IR region. Upon reduction to the −1 state, new broad bands appear. The −1 state of **1** (hereafter designated as $\mathbf{1}^-$) shows strong low-energy absorption bands at $\tilde{\nu}_{max} = 12\,100$ cm^{-1} ($\epsilon = 13\,100$ M^{-1} cm^{-1}) and $\tilde{\nu}_{max} = 6700$ cm^{-1} ($\epsilon = 9370$ M^{-1} cm^{-1}). The −2 state of **1** shows an intense broad band with a shoulder at shorter wavelength at $\tilde{\nu}_{max} = 7140$ cm^{-1} ($\epsilon = 17\,900$ M^{-1} cm^{-1}). Since cluster-to-cluster intervalence charge transfer (ICT) should appear only in the −1 state ($Ru_3^{III,III,II}$-pz-$Ru_3^{III,II,II}$), the band at $\tilde{\nu}_{max} = 12\,100$ cm^{-1} is assigned to be the ICT absorption of $\mathbf{1}^-$. The band at $\tilde{\nu}_{max} = 6700$ cm^{-1} may be assigned to intracluster CT transition(s) within the $Ru_3^{III,II,II}$ unit. We note that the −2 state also exhibits a band at nearly the same energy with double intensity. Significantly, the unbridged cluster anion $[Ru_3^{III,II,II}(\mu_3\text{-}O)(CH_3COO)_6(CO)(dmap)_2]^-$ [17] also shows a band with a shoulder on the high energy side, very similar to that observed at $\tilde{\nu}_{max} = 7140$ cm^{-1} for the −2 state of **1**. These facts support the assignments of intercluster ICT absorption at $\tilde{\nu}_{max} = 12\,100$ cm^{-1} and intracluster absorption at 6700 cm^{-1}. Complexes **2** and **3** show very similar spectral changes, upon

(12) Sutton, J. E.; Taube, H. *Inorg. Chem.* **1981**, *20*, 3125.
(13) de la Rosa, R.; Chang, P. J.; Salaymeh, F.; Curtis, J. C. *Inorg. Chem.* **1985**, *24*, 4229.
(14) Dong, Y.; Hupp, J. T. *Inorg. Chem.* **1992**, *31*, 3170.
(15) Lacoste, M.; Rabaâ, G.; Astruc, D.; Ardoin, N.; Varret, G.; Saillard, J.-Y.; LeBeuze, A. *J. Am. Chem. Soc.* **1990**, *112*, 9548.

(16) These compounds were prepared in a similar way to **1**−**6**. Redox data: $E_{1/2}(+4/+2) = +1.17$ (L = dmap), +1.30 (L = py), +1.32 (L = cpy); $E_{1/2}(+2/0) = +0.44$ (L = dmap), +0.51 (L = py), +0.54 (L = cpy) V vs SSCE and $E_{1/2}(0/-2) = -1.31$ (L = dmap), −1.15 (L = py), −0.94 (L = cpy) V vs SSCE.

Table 2. Summary of Electronic Spectral Data for the ICT Bands of the Mixed Valence (−1) State of $\{[Ru_3(\mu_3\text{-}O)(\mu\text{-}CH_3CO_2)_6((CO)(L)]_2(\mu\text{-}pz)\}^{1-}$ [a]

	L	$\tilde{\nu}_{max}$ (cm^{-1})	ϵ_{max} ($M^{-1}\,cm^{-1}$)	$\Delta\tilde{\nu}_{1/2}$ (cm^{-1})	H_{AB} (cm^{-1})
1	dmap	12100	12200	3760	2180
2	py	11800	10700	3930	2060
3	cpy	10800	6610	5220	1310

[a] Data at −10 °C.

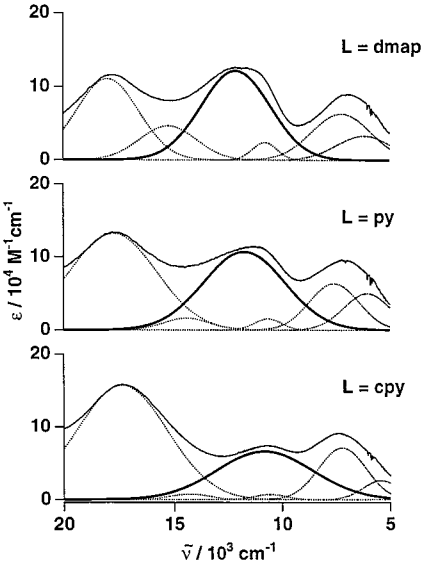

Figure 4. Electronic absorption spectal data for **1** (top), **2** (middle), and **3** (bottom) in the 1-electron reduced ($n = -1$) states in dichloromethane, −10 °C (solid line), and the deconvoluted ICT band (dotted line). The solid bold line corresponds to the single Gaussian fit of the ICT band.

reduction, and similar ICT band assignments can be made (Table 2).

Intercluster electronic coupling, H_{AB}, was estimated by deconvolution of the ICT spectra of $\mathbf{1}^-$−$\mathbf{3}^-$ (Figure 4). Reasonably good agreement between the observed spectra of $\mathbf{1}^-$, $\mathbf{2}^-$, and $\mathbf{3}^-$ and the sum of deconvoluted spectral components was obtained. It was assumed that the ICT band consists of a single Gaussian band shape and that the intracluster transitions at longer wavelength have three components. Figure 4 and Table 2 summarize spectral data extracted from the ICT band shape analysis. On going from $\mathbf{1}^-$ to $\mathbf{3}^-$, that is, as we go to progressively less strongly interacting systems, the ICT band positions shift from higher to lower energy. Concomitantly, the band intensities decrease and the bands broaden significantly as reflected in the band half-widths. The systematic trends are consistent with theoretical predictions for ICT band shape in strongly coupled systems.[19] Salaymeh et al. report a systematic decrease in $\Delta\tilde{\nu}_{1/2}$ as $\Delta E_{1/2}$ increases in a series of symmetric pz-bridged Ru^{3+}/Ru^{2+} intervalence complexes.[20] A very similar trend is observed here for compounds $\mathbf{1}^-$−$\mathbf{3}^-$ (Tables 1 and 2).

The electronic coupling H_{AB}, derived from the optical spectra of the singly reduced (−1) charge-transfer states, is given by eq 3.[19]

$$H_{AB} = (2.05 \times 10^{-2})(\tilde{\nu}_{max}\epsilon_{max}\Delta\tilde{\nu}_{1/2})^{1/2}/r \qquad (3)$$

Optical estimates of H_{AB}[21] range by nearly a factor of 2 from 2180 ($\mathbf{1}^-$) to 1310 cm^{-1} ($\mathbf{3}^-$). In the Robin−Day classification of intervalence charge-transfer complexes,[22] $\mathbf{3}^-$ can be considered to be a largely charge localized Class II complex, based on $\Delta\tilde{\nu}_{1/2}$. According to a Hush analysis of intervalence charge-transfer bands,[19] the expected half widths of the intervalence charge-transfer (ICT) bands in the mixed valence (−1) states are $\Delta\tilde{\nu}_{1/2}$(calc) = 5290 cm^{-1} for $\mathbf{1}^-$, 5220 cm^{-1} for $\mathbf{2}^-$, and 4990 cm^{-1} for $\mathbf{3}^-$. Comparison of these values with the experimentally observed data in Table 2 indicates that $\mathbf{1}^-$ and $\mathbf{2}^-$ go beyond Robin−Day criteria[22] for Class II behavior and approach Class III (delocalized), whereas $\mathbf{3}^-$ conforms to Class II behavior. We were unable to observe the ICT bands in the −1 states of **4**−**6** owing to the experimental difficulties of working within small ΔE windows and the broad, weak bands expected in the less strongly coupled systems.

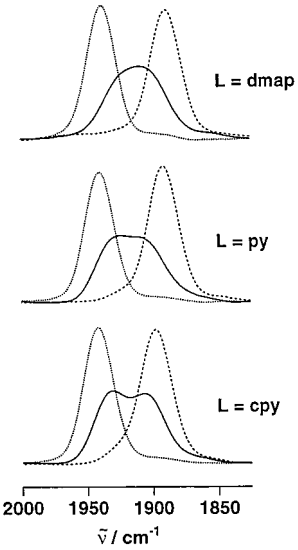

Figure 5. Infrared spectra for $[\{Ru_3(\mu_3\text{-}O)(\mu\text{-}CH_3CO_2)_6(CO)(L)\}_2(\mu\text{-}pz)]^n$ ($n = 0$ (···), −1 (—), −2 (- - -) in 0.1 M tetra-*n*-butylammonium hexaflurophosphate dichloromethane solution for **1** (top), **2** (middle), and **3** (bottom).

Reflectance Infrared Spectroelectrochemistry of 1−6. The vibrational spectra of complexes **1**−**6** were obtained by using reflectance IR spectroelectrochemistry (SEC). Controlled potentials were applied to prepare the singly (−1) and doubly (−2) reduced states of clusters **1**−**6** for IR spectroscopic observation. In the isolated (0) state, **1** (L = dmap) exhibits a single ν(CO) band at 1938 cm^{-1} (Figure 5 (top)). The normal modes associated with C−O stretching of the carbon monoxide ligands

(17) $[Ru_3^{III,III,II}(\mu_3\text{-}O)(CH_3COO)_6(CO)(dmap)_2]$ was prepared similarly to $[Ru_3^{III,III,II}(\mu_3\text{-}O)(CH_3COO)_6(CO)(py)_2]$.[18] Anal. Calcd for $Ru_3C_{27}H_{38}O_{14}N_4$: C, 34.29, H, 4.05, N, 5.92. Found: C, 33.96, H, 4.12, N, 5.87. ^1H NMR (270 MHz, $CDCl_3$) 9.01 (4H, dmap-*o*), 7.23 (4H, dmap-*m*), 3.32 (12H, dmap CH_3), 2.03 (12H, acetate CH_3), 1.76 (6H, acetate CH_3) ppm.

(18) Baumann, J. A.; Wilson, S. T.; Salmon, D. J.; Hood, P. L.; Meyer, T. J. *J. Am. Chem. Soc.* **1979**, *101*, 2916.

(19) Hush, N. S. *Prog. Inorg. Chem.* **1967**, *8*, 391.

(20) Salaymeh, F.; Berhane, S.; Yusof, R.; de la Rosa, R.; Fung, E. Y.; Matamoros, R.; Law, K. W.; Zheng, Q.; Kober, E. M.; Curtis, J. C. *Inorg. Chem.* **1993**, *32*, 3895.

(21) H_{AB} is a function of r (see eq 3). CV behavior of **1**−**3** and related compounds show that r is not the same depending on the electron-donating or -withdrawing nature of the terminal ligand. Although the "$Ru_3(\mu_3\text{-}O)$" core has a delocalized electronic structure, the first electron in the reduction of **1** goes into the LUMO, which consists mainly of the d-orbital of the Ru atoms bound directly to the pz nitrogen. On the other hand, in the reduction of **3**, the first electron goes into LUMO, to which d-orbitals of both Ru atom bound to pz and cpy contribute significantly. Therefore, H_{AB}'s for **1** and **2** were estimated with use of the shortest Ru−Ru distance (7.02 Å based on X-ray data), whereas H_{AB} for **3** was estimated by averaging weighted H_{AB}'s for all the possible Ru−Ru separations ($H_{AB} = 0.25H_{AB}$ (r = 7.02 Å) + $0.125H_{AB}$ (r = 12.76 Å) + $0.5H_{AB}$ (r = 10.05 Å) + $0.125H_{AB}$ (r = 13.16 Å)). H_{AB} for **2**, therefore, may be slightly overestimated and gives the maximum limit.

(22) Robin, M. B.; Day, P. *Adv. Inorg. Chem. Radiochem.* **1967**, *10*, 247.

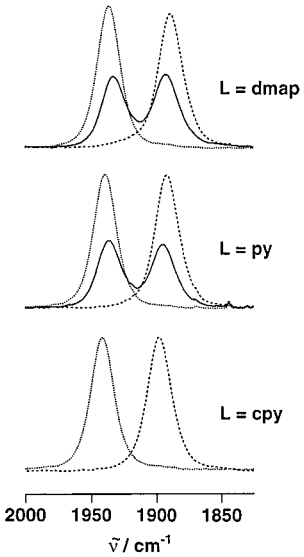

Figure 6. Infrared spectra for $[\{Ru_3(\mu_3\text{-}O)(\mu\text{-}CH_3CO_2)_6(CO)(L)\}_2(\mu\text{-bpy})]^n$ ($n = 0$ (···), -1 (—), -2 (- - -) in 0.1 M tetra-*n*-butylammonium hexaflurophosphate dichloromethane solution for **4** (top), **5** (middle), and **6** (bottom).

on each $Ru_3^{III,III,II}$ unit contribute to a single ν(CO) band due to their identical local environments and large spatial separation. The doubly reduced species also gives rise to a single ν(CO) band, but at 1889 cm^{-1}, reflecting identical redox states at each $Ru_3^{III,II,II}$ cluster. Complexes **2** and **3** similarly exhibit single ν(CO) bands in the neutral state and -2 state, respectively. In view of these results it is reasonable to expect that the single-electron-reduced state of **1** will show two ν(CO) bands, one characteristic of a $Ru_3^{III,III,II}$ environment and the other characteristic of $Ru_3^{III,II,II}$. However, for the -1 state of **1**, two ν(CO) bands are not observed. Rather, a broad absorption band at the average energy of the bands observed for the neutral (0) and doubly reduced (-2) states of **1** is seen (Figure 5 (top)). The degree of "coalescence" of the IR spectra depends on the degree of electronic coupling between the pyrazine-linked Ru_3 clusters (Figure 5). As H_{AB} decreases from 2180 cm^{-1} for **1** to 1310 cm^{-1} (optical values) for **3**, two distinct ν(CO) bands at 1931 and 1904 cm^{-1} become resolved for **3**. Cluster **2** with an intermediate value of H_{AB} of 2060 cm^{-1}, shows an intermediate degree of spectral "coalescence" in the singly reduced state.

Similarly, both the neutral and -2 states of the bpy-bridged complexes **4**$-$**6** exhibit one sharp ν(CO) band in the IR (Figure 6). The spectra of the -1 states of **4**$-$**5** consist of two well-resolved and well-separated ν(CO) bands, perturbed only slightly relative to the spectra of the neutral and -2 states. Careful analysis for **4** suggests that a small amount of broadening may be occurring (vide infra). For **6**, a reliable spectrum of the -1 state could not be obtained due to <50 mV separation between (0/$-$1) and ($-$1/$-$2) CV waves. In clusters **4**$-$**6** the electronic coupling is small as evidenced by cyclic voltammetry (vide supra). Overall, the singly reduced states of **4**$-$**6** can be viewed as valence trapped or localized compounds, and classified as Class II in the Robin$-$Day classification scheme.

The main point of the comparison of the IR spectra in the ν(CO) region of the -1 states of **1**$-$**3** to those of **4**$-$**6** is to show the differences in spectral characteristics that arise from the electronic interactions. The mixed valence states of **1**$-$**3** show clear evidence of strong electronic coupling in their electrochemistry and optical spectra. The use of longer bpy bridges in **4**$-$**6** attenuates electronic coupling to the point that in **6** the -1 charge-transfer state is no longer defined. In simple terms, the strongly interacting Ru_3 centers of the -1 states of **1**$-$**3** have extensively "mixed" IR spectral features, quite different from the neutral and -2 state spectra. The weakly coupled systems **4** and **5** show essentially independent ν(CO) IR spectral features in the -1 state, quite similar to those observed in the neutral and -2 states. It is striking that the "mixing" of the IR spectral line shape of the ν(CO) bands of the -1 states tracks the electronic mixing. The relationship between electron-transfer dynamics and electronic coupling is quite well understood. This study establishes a relationship between electronic coupling in a charge-transfer complex and IR spectral line shape. However, the exact way that the IR spectral line shape relates to the system dynamics remains to be clarified. It is interesting to consider the differences in IR line shapes of **1**$-$**3** and **4**$-$**6** in light of ideas recently expressed by Turner and co-workers,[23] and by Strauss and co-workers.[1,24$-$26] In essence, Turner and co-workers favor a dynamical model where Bloch-type equations apply. Here, the dynamic exchange occurs by interwell dynamics, in effect two-site hopping. Strauss and co-workers have pointed out that many dynamical effects observed in infrared spectra are attributable to relaxation processes occurring within a single potential energy well. Intrawell dynamics can produce "pseudo collapse" of two bands that broaden to become one. Turner discusses a significant difference in the spectroscopy of intrawell vs interwell (exchanging) systems. This is the "exchange intensity", a buildup of intensity at the average energy of the two exchanging spectral components. The "exchange intensity" is contributed in excess of what would be expected from the simple superposition of two bands.[23] It is a normal consequence of dynamic exchange processes when Bloch equations apply.[27] Turner suggests that the presence of extra "exchange" intensity is a crucial signature of interwell exchange. This extra contribution to the line shape is not expected from the intrawell dynamical model.[25]

At the present time, we have no evidence of a process other than intramolecular electron transfer to account for the changes observed in the IR spectral line shapes of our systems. We have therefore limited our treatment of the data to the NMR-like Bloch equation analysis. The Bloch-type line shape analysis was used by Grevels and Turner to study the IR band broadening in $Fe(CO)_3$(NBD) (NBD = norbornadiene).[23,28,29] Cannon and co-workers estimated the rate of electron transfer in $[Fe^{III}_2Fe^{II}O(OOCMe)_6(py)_3]$ from the appearance of the IR spectral line shape of the $\nu_{as}(Fe_3O)$ bands in the mixed valence state.[30] Cannon's work is the only study of the applicability of the Bloch-type analysis to IR spectral line broadening due to electron transfer. We follow the Bloch equation type analysis developed by McClung.[29] Figure 7 shows the simulated spectral line shapes as a function of k_e and a comparison to the observed spectra of **1**$-$**3**. The rates of electron transfer estimated by this type of simulation for $\mathbf{1}^-$, $\mathbf{2}^-$, and $\mathbf{3}^-$ are $9 \pm 3 \times 10^{11}$, $5 \pm 3 \times 10^{11}$, and ca. 1×10^{11} s^{-1}, respectively. For $\mathbf{1}^-$, this rate constant allows estimation of the activation energy for electron

(23) Turner, J. J.; Gordon, C. M.; Howdle, S. M. *J. Phys. Chem.* **1995**, *99*, 17532.
(24) Wood, K. A.; Strauss, H. L. *Ber. Bunsen-Ges. Phys. Chem.* **1989**, *93*, 615.
(25) Strauss, H. L. *J. Am. Chem. Soc.* **1992**, *114*, 905.
(26) MacPhail, R. A.; Strauss, H. L. *J. Chem. Phys.* **1985**, *82*, 1156.
(27) Sandström, J. *Dynamic NMR Spectroscopy*; Academic Press: London, 1982.
(28) Grevels, F.-W.; Jacke, J.; Klotzbücher, W. E.; Krüger, C.; Seevogel, K.; Tsay, Y. H. *Angew. Chem., Int. Ed. Engl.* **1987**, *26*, 885.
(29) Grevels, F.-W.; Kerpen, K.; Klotzbücher, W. E.; McClung, R. E. D.; Russel, G.; Viotte, M.; Schaffner, K. *J. Am. Chem. Soc.* **1998**, *120*, 10423.
(30) Wu, R.; Arap Koske, S. K.; White, R. P.; Anson, C. E.; Jayasooriya, U. A.; Cannon, R. D. *J. Chem. Soc., Chem. Commun.* **1994**, 1657.

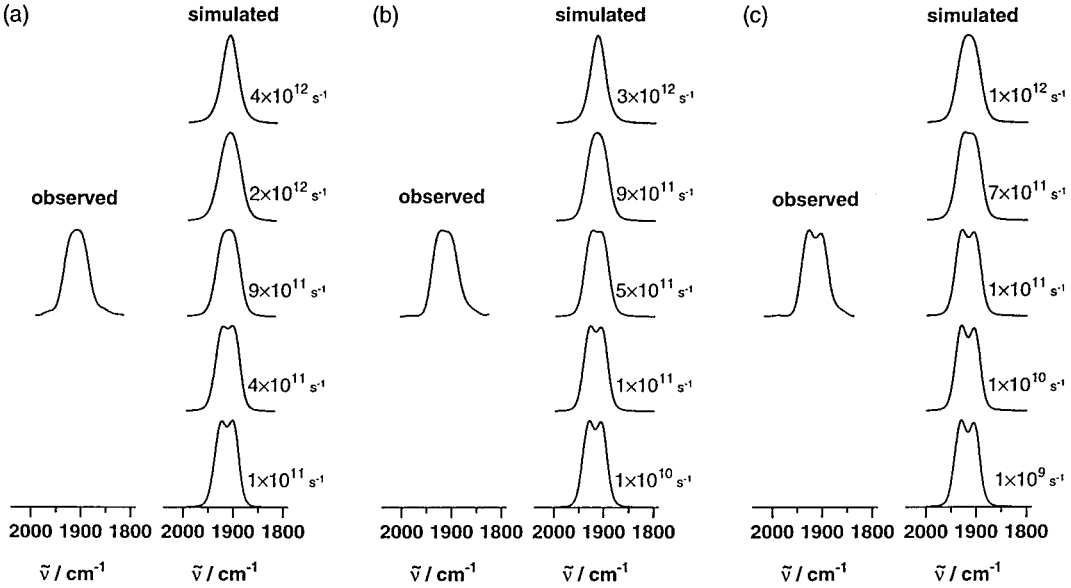

Figure 7. Comparison of observed to simulated infrared spectra for the mixed valence state of **1** (a), **2** (b), and **3** (c) as a function of the intramolecular electron-transfer rate constant, k_e.

transfer at 1 kcal/mol. This compares with the ca. 35 kcal/mol (12 100 cm^{-1}) splitting between the upper and lower potential energy surfaces. Clearly **1** is at the threshold of intrawell behavior with a ground-state potential energy surface characterized by a "bump" of less than 2*k*T in the middle of a single well. The spectral line shape simulation for $\mathbf{3}^-$ (Figure 7c) gives k_e = ca. 1×10^{11} s^{-1}, which is clearly less than the rate constants estimated for $\mathbf{1}^-$ and $\mathbf{2}^-$. Simulated spectra as a function of k_e for $\mathbf{3}^-$ also show that k_e for $\mathbf{3}^-$ is very close to the lower limit that can be determined reliably by this approach. Figure 7 also shows that at a rate constant $k_e = 10^{11}$ s^{-1}, two distinct spectral features are resolved, and this could be considered "slow exchange" on the IR time scale.

Are the rate constants estimated from the Bloch-type treatment consistent with expectations? The −1 state of complex **3** is a Robin−Day class II complex, and thus its electron-transfer rate constant can be independently estimated from Marcus theory. By making typical assumptions ($\kappa = 1$, $\nu_n = 5 \times 10^{12}$ s^{-1}, $\Delta G_\lambda^* = \tilde{\nu}_{max}/4$), the rate constant for exchange of $k_e = 1 \times 10^9$ s^{-1} at 263 K for $\mathbf{3}^-$ is estimated from eq 1, using data from the ICT spectrum (Table 2). This is smaller by 2 orders of magnitude than the rate constant estimated from the IR line shape simulation. The underestimation of k_e based on the ICT band data and eqs 1 and 3 may arise from two factors: (i) The value of *r* used in eq 3 for the calculation of H_{AB} for $\mathbf{3}^-$ [21] might be shorter than assumed (10.02 Å). A shorter *r* value gives a larger H_{AB} and hence a larger k_e. (ii) The detailed electronic structure of $\mathbf{3}^-$ may lie beyond the region where eq 1 is applicable. An independent means of distinguishing electronically localized vs delocalized systems is based on the IR spectra of the bridging pyrazine modes. It has been often argued that in a mixed valence state of a pyrazine-bridged dimer the appearance of a symmetric ν(pz) band at 1580−1590 cm^{-1} provides evidence for valence localization (class II), while a fully delocalized class III system does not show the ν(pz) band.[31−34] In the present case, it was not possible to discuss the degree of delocalization based on the intensity of the ν(pz) band, because the acetate ligand $\nu(COO)_{asym}$ bands obscure the ν(pz) band.[32] Recently Meyer et al. pointed out the difficulty in the discrimination between localization and delocalization from the presence or the absence of ν(pz).[34]

One way to view the limits on the exchange rate constants is to consider the slowest motions that render the two CO oscillators equivalent. In the −1 states the symmetric charge-transfer complexes can be viewed as having two ground-state equilibrium C−O bond distances in the localized limit. This results from the usual back-bonding effects on ground-state C−O bond distance and ν(CO). In the delocalized limit, there is one equilibrium C−O bond distance for both CO ligands, and one ν(CO) band. As the C−O bond distances adjust to charge transfer from one side of the complex to the other, it is clear that the fastest time that the adjustments can be made is on the order of a few periods of vibration of the relevant mode. For the ν(CO) modes this would be on the order of 5×10^{13} s^{-1}. However, as always, the rate will be limited by the slowest modes, and here it is likely that the Ru−N(pz) or Ru−CO vibrations come into play. These are in the 400 cm^{-1} range, corresponding to rates on the order of 1×10^{13} s^{-1}. The maximum rate constants to be expected from this simple argument are about an order of magnitude higher than those estimated from the Bloch-type analysis of the IR line shapes for the pz-bridged dimers $\mathbf{1}^-$, $\mathbf{2}^-$, and $\mathbf{3}^-$. These line shape simulations, however, show that while coalescence appears to be occurring for $\mathbf{1}^-$ and nearly occurring for $\mathbf{2}^-$ and $\mathbf{3}^-$, these systems are by no means in a fast exchange regime. Thus, the Bloch-type analysis does predict rate constants that at least are consistent with other physical considerations. In fact, we believe that the rate constants estimated by IR band shape analysis are more reliable than those obtained from the ICT band analysis, because they are based on a direct physical measurement.

Finally, we return to the issue of "exchange intensity" which is accumulated at the average energy of the two exchanging spectral features, as discussed by Turner. In comparison to the most rapidly exchanging systems **1**−**3**, the IR spectra of the weakly coupled systems **4**−**6** show relatively little intensity

(31) Callahan, R. W.; Keene, F. R.; Meyer, T. J.; Salmon, D. J. *J. Am. Chem. Soc.* **1977**, *99*, 1064.

(32) Baumann, J. A.; Salmon, D. J.; Wilson, S. T.; Meyer, T. J.; Hatfield, W. E. *Inorg. Chem.*, **1978**, *17*, 3342.

(33) Hornung, F. M.; Baumann, F.; Kaim, W.; Olabe, J. A.; Slep, L. D.; Fiedler, J. *Inorg. Chem.*, **1998**, *37*, 311−316.

(34) Demadis, K. D.; Neyhart, G. A.; Kober, E. M.; Meyer, T. J. *J. Am. Chem. Soc.* **1998**, *120*, 7121−7122.

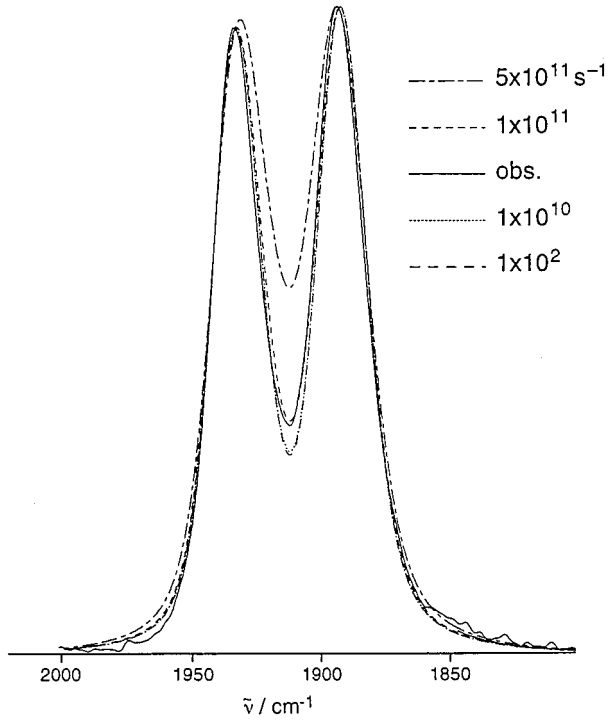

Figure 8. Comparison of the corrected experimental IR spectrum of $\mathbf{4}^-$ (solid line) to simulated spectra assuming rate constants $k_e = 1 \times 10^2$, 1×10^{10}, 1×10^{11}, and 5×10^{11} s^{-1}. Spectral correction involved subtracting the expected thermodynamic contributions of ca. 8.3% of **4** and $\mathbf{4}^{2-}$ to the overall spectrum.

between the high- and low-energy features in the −1 states. Nonetheless, rates of intramolecular electron transfer in the bpy-bridged systems **4**−**6** are expected to be rapid, although not so rapid as to be clearly observed in the vibrational spectra. It is thus useful to examine the limits of the IR spectral simulation method of determining intramolecular electron-transfer rate constants from IR spectra, and the possible presence of "exchange intensity" in the spectra of **4**−**6**. We consider only the case of $\mathbf{4}^-$ since it is expected to be the fastest of the bpy-bridged systems. The electrochemical splitting ΔE observed in the CV of **4** is 120 mV, corresponding to a comproportionation constant $K_c = 110$ (Table 1). The IR spectrum of $\mathbf{4}^-$ then must envelop spectral components of **4**, $\mathbf{4}^-$, and $\mathbf{4}^{2-}$ in the approximate ratio 1:10:1. Since the overlap of intensity from the bands attributed to **4** and $\mathbf{4}^{2-}$ contributes intensity to the mid-energy point of the spectrum of $\mathbf{4}^-$, the spectrum was corrected for these contributions before simulation. Figure 8 compares the corrected IR spectrum of $\mathbf{4}^-$ to simulated spectra assuming rate constants k_e varying from 1×10^2 to 5×10^{11} s^{-1}. This comparison suggests that k_e for $\mathbf{4}^-$ could be faster than 1×10^{10} s^{-1} and still give a largely nonoverlapped IR spectrum. The comparison also shows that for rate constants below ca. 1×10^{11} s^{-1}, the reliability of the IR spectral simulation method becomes limited. The Bloch type analysis gives physically reasonable estimates of the rate constants for exchange in these systems, and predicts the presence of "exchange intensity" in the spectrum of $\mathbf{4}^-$.

Conclusions

Uncertainties in the rates of electron transfer estimated by Bloch equation simulation of the IR band shape exist, but the rate constants obtained for $\mathbf{1}^-$−$\mathbf{3}^-$ are reasonable within the context of theories of electron transfer. The correlation of IR line shape for the mixed valence states of **1**−**6** with electronic coupling H_{AB} provides convincing evidence of the effects of intramolecular electron transfer on the time scale of observation by IR spectroscopy ($<10^{-11}$ s). The precise relationship between IR line shape and electron-transfer dynamics still needs to be refined, but systems such as those reported here offer great advantages for tuning electron-transfer rate to limits near the maximum possible, and for comparing theory and experiment.

Experimental Section

Materials. All solvents were dried with appropriate agents. Acetonitrile (Fisher) was distilled from the CaH_2. Dichloromethane was distilled over CaH_2. TBAH (tetrabutylammonium hexafluorophosphate) was received from Aldrich, recrystallized from hot dry ethanol, and dried in vacuo at 170 °C for 48 h.

Preparation of 1−3. These compounds were prepared as described previously.[4]

Preparation of 4−6. The bpy-bridged compounds, **4**−**6**, were prepared similarly to **1**−**3** by reacting equal molar quantities of $Ru_3(\mu_3\text{-O})(\mu\text{-CH}_3CO_2)_6(CO)(L)(H_2O)$ (see below) and $Ru_3(\mu_3\text{-O})(\mu\text{-CH}_3CO_2)_6(CO)(L)(bpy)$ (see below). The dmap complex (**4**) was prepared as follows. A mixture of $Ru_3(\mu_3\text{-O})(\mu\text{-CH}_3CO_2)_6(CO)(dmap)(H_2O)$ (51 mg, 0.061 mmol) and $Ru_3(\mu_3\text{-O})(\mu\text{-CH}_3CO_2)_6(CO)(dmap)(bpy)$ (54 mg, 0.055 mmol) in CH_2Cl_2 (10 mL) was allowed to stand for 3 days at room temperature. The resulting solution was chromatographed over silica gel (Wakogel C-200, column length = 13 cm, column diameter = 2 cm) with CH_2Cl_2/EtOH 100:2 (volume/volume) as the eluting agent. The compound was isolated from the second blue-green main band. Yield 77 mg. **5** and **6** were prepared in a similar way with the use of py or cpy derivatives. For **4**. Anal. Calcd for $Ru_6C_{50}H_{64}O_{28}N_6$: C, 33.30; H, 3.58; N, 4.66. Found: C, 32.88; H, 3.77; N, 4.57. FABMS: *m*/*z* 1776 (calcd (M − CO) = 1776). ^{1}H NMR (270 MHz, $CDCl_3$) 9.34 (4H, bpy-*o*), 8.97 (4H, dmap-*o*), 8.50 (4H, bpy-*m*), 7.23 (4H, dmap-*m*), 3.33 (12H, dmap CH_3), 2.14 (12H, acetate CH_3), 2.10 (12H, acetate CH_3), 1.88 (12H, acetate CH_3) ppm. For **5**. Anal. Calcd for $Ru_6C_{46}H_{54}O_{28}N_4$: C, 32.17, H, 3.17; N, 3.26. Found: C, 32.50; H, 3.28; N, 3.40. FABMS: *m*/*z* 1690 (calcd (M − CO) = 1689). ^{1}H NMR (270 MHz, $CDCl_3$) 9.30 (4H, bpy-*o*), 9.08 (4H, py-*o*), 8.48 (4H, bpy-*m*), 8.20 (2H, py-*p*), 8.06 (4H, py-*m*), 2.18 (12H, acetate CH_3), 2.14 (12H, acetate CH_3), 1.92 (12H, acetate CH_3) ppm. For **6**. Anal. Calcd for $Ru_6C_{48}H_{52}O_{28}N_6$: C, 32.62; H, 2.97; N, 4.76. Found: C, 32.34; H, 3.10; N, 4.67. FABMS: *m*/*z* 1741 (calcd (M − CO) = 1739). ^{1}H NMR (270 MHz, $CDCl_3$) 9.16 (4H, bpy-*o*), 8.88 (4H, cpy), 8.44 (4H, bpy-*m*), 8.20 (4H, cpy), 2.16 (12H, acetate CH_3), 2.14 (12H, acetate CH_3), 1.93 (12H, acetate CH_3) ppm.

Preparation of $Ru_3(\mu_3\text{-O})(\mu\text{-CH}_3CO_2)_6(CO)(L)(H_2O)$ (L = dmap and cpy). These complexes were prepared in a similar way to the corresponding pyridine derivative $Ru_3(\mu_3\text{-O})(\mu\text{-CH}_3CO_2)_6(CO)(py)(H_2O)$[6] with use of dmap or cpy in place of py. For $Ru_3(\mu_3\text{-O})(\mu\text{-CH}_3CO_2)_6(CO)(dmap)(H_2O)\cdot 4H_2O$. Anal. Calcd for $Ru_3C_{20}H_{38}O_{19}N_2$: C, 26.29; H, 4.19; N, 3.07. Found: C, 26.39; H, 3.85; N, 3.37. ^{1}H NMR (270 MHz, D_2O−DCl, vs TSP) 9.10 (2H, dmap-*o*), 7.43 (2H, dmap-*m*), 3.30 (6H, dmap CH_3), 1.95 (6H, acetate CH_3), 1.94 (6H, acetate CH_3), 1.92 (6H, acetate CH_3) ppm. For $Ru_3(\mu_3\text{-O})(\mu\text{-CH}_3CO_2)_6(CO)(cpy)(H_2O)\cdot 2H_2O$. Anal. Calcd for $Ru_3C_{19}H_{28}O_{17}N_2$: C, 26.54; H, 3.28; N, 3.26. Found: C, 26.72; H, 3.28; N, 3.42. ^{1}H NMR (270 MHz, CD_3CN) 9.10 (2H, cpy), 8.37 (2H, cpy), 2.03 (6H, acetate CH_3), 2.01 (6H, acetate CH_3), 1.83 (6H, acetate CH_3) ppm.

Preparation of $[Ru_3(\mu_3\text{-O})(\mu\text{-CH}_3CO_2)_6(CO)(L)(bpy)]$ (L = dmap, py, cpy). $[Ru_3(\mu_3\text{-O})(\mu\text{-CH}_3CO_2)_6(CO)(dmap)(bpy)]$ was prepared as follows. A mixture of $[Ru_3(\mu_3\text{-O})(\mu\text{-CH}_3CO_2)_6(CO)(dmap)(H_2O)]$ (100 mg, 0.119 mmol) and 4,4′-bipyridine (188 mg, 1.20 mmol) in CH_2Cl_2 (15 mL) was stirred for 3 days at room temperature. The resulting solution was chromatographed over silica gel (Wakogel C-200, column length = 11 cm, column diameter = 3 cm) with $CHCl_3/C_2H_5OH$ 100:2 (volume/volume) as the eluting agent. The compound was isolated from the second blue-green main band. Yield 88 mg. The py and cpy derivatives were prepared in a similar way. For $[Ru_3(\mu_3\text{-O})(\mu\text{-CH}_3CO_2)_6(CO)(dmap)(bpy)]$. Anal. Calcd for $Ru_3C_{30}H_{36}O_{14}N_4$: C, 36.77; H, 3.70; N, 5.72. Found: C, 36.50; H, 3.81; N, 5.69. FABMS: *m*/*z* 953 (calcd (M − CO) = 952). ^{1}H NMR (270 MHz, $CDCl_3$) 9.20 (2H, coord bpy-

o), 8.96 (2H, dmap-*o*), 8.91 (2H, uncoord bpy-*o*), 8.27 (2H, coord bpy-*m*), 7.80 (2H, uncoord bpy-*m*), 7.22 (2H, dmap-*m*), 3.31 (6H, dmap CH_3), 2.09 (6H, acetate CH_3), 2.08 (6H, acetate CH_3), 1.82 (6H, acetate CH_3) ppm. For $[Ru_3(\mu_3\text{-}O)(\mu\text{-}CH_3CO_2)_6(CO)(py)(bpy)]$. Anal. Calcd for $Ru_3C_{28}H_{31}O_{14}N_3$: C, 35.90; H, 3.34; N, 4.49. Found: C, 35.94; H, 3.46; N, 4.60. FABMS: *m*/*z* 910 (calcd (M − CO) = 909). ^{1}H NMR (270 MHz, $CDCl_3$) 9.13 (2H, coord bpy-*o*), 9.06 (2H, py-*o*), 8.90 (2H, uncoord bpy-*o*), 8.27 (2H, coord bpy-*m*), 8.18 (1H, py-*p*), 8.04 (2H, py-*m*), 7.79 (2H, uncoord bpy-*m*), 2.12 (6H, acetate CH_3), 2.10 (6H, acetate CH_3), 1.87 (6H, acetate CH_3) ppm. For $[Ru_3(\mu_3\text{-}O)(\mu\text{-}CH_3CO_2)_6(CO)(cpy)(bpy)]$. Anal. Calcd for $Ru_3C_{29}H_{30}O_{14}N_4$: C, 36.22; H, 3.14; N, 5.83. Found: C, 36.13; H, 3.11; N, 5.47. FABMS: *m*/*z* 935 (calcd (M − CO) = 934). ^{1}H NMR (270 MHz, $CDCl_3$) 9.02 (2H, coord bpy-*o*), 8.92 (2H, cpy), 8.90 (2H, uncoord bpy-*o*), 8.26 (2H, coord bpy-*m*), 8.21 (2H, cpy), 7.78 (2H, uncoord bpy-*m*), 2.13 (6H + 6H, acetate CH_3), 1.91 (6H, acetate CH_3) ppm.

Cyclic Voltammetry of 1−6. All cyclic voltammetry experiments were carried out by using a BAS CV-50W Voltammetric Analyzer at a scan rate of 100 mV/s. The working electrode was glassy carbon. The counter electrode was a platinum coil, and the reference electrode was a saturated sodium calomel electrode, SSCE. In all cases, 0.1 M solutions of tetrabutylammonium hexafluorophosphate (TBAH) in dichloromethane were used.

Reflectance Infrared Spectroelectrochemistry. IR spectral changes accompanying thin-layer bulk electrolyses were measured by using a modified[35] temperature-controlled flow-through reflectance spectroelectrochemical cell reported earlier.[36] Path lengths were typically 0.05 mm. The controlled potentials were measured vs an Ag pseudoreference electrode (ca. −0.06V vs SCE). Spectroelectrochemical experiments were carried out in 0.1 M tetra-*n*-butylammonium hexafluorophosphate solutions with freshly distilled dichloromethane. All solutions were prepared under an atmosphere of nitrogen and deoxygenated completely by N_2 gas before injection into the SEC cell. Blank reference solutions containing 0.1 M tetra-*n*-butylammonium hexafluorophosphate were used for the Fourier Transform IR solvent subtractions. In some cases, spectral baseline shifts in the different redox states were adjusted. All measurements were performed at room temperature. A Princeton Applied Research (PAR) Model 175 Universal Programmer with a PAR Model 176 Current Follower were used to effect and monitor thin layer bulk electrolyses. The IR spectra were acquired with use of a Mattson Research Series 1 Fourier Transform IR equipped with a liquid nitrogen cooled MCT (mercury−cadmium−telluride) detector.

Intervalence Charge-Transfer Spectra. Controlled-potential absorption spectra were obtained with an optically transparent thin-layer electrode (OTTLE) cell (light path length = 0.5 mm). The working and the counter electrodes were platinum mesh and platinum coil, respectively. The potential was applied with a Hokuto-Denko potentio/galvanostat, model HA-501, and referred to an SSCE (saturated sodium chloride calomel electrode). The spectra were measured with a Shimadzu UV-3100 PC spectrophotometer. All spectroelectrochemical measurements were carried out at ca −10 °C under a nitrogen atmosphere.

Simulation of Infrared Line Shape for Exchanging Spectra. IR spectral line shapes were simulated by using the dynamical simulation program VIBEXGL: Program for the Simulation of IR Spectra of Exchanging Systems, made available by Prof. R. E. D. McClung, University of Alberta.[29]

Acknowledgment. This work was supported by NSF grant (CHE-9615886) to C.P.K. and Grants-in-Aid for Scientific Research (No. 09874128 and Priority Area No. 10149102) from the Ministry of Education, Science, and Culture and a grant from Monbusho International Scientific Research Program (No. 09044054) (Japan) to T.I. A Japan Society for the Promotion of Science for fellowship support to C.P.K., NSERC (Canada) for a postdoctoral fellowship to J.W., and the Purdue Research Foundation for a fellowship to I.S.Z. are also gratefully acknowledged.

JA984000Z

(35) Zavarine, I. S.; Richmond, T. A.; Kubiak, C. P. *J. Electroanal. Chem.* Submitted for publication.

(36) Wittrig, R. E.; Kubiak, C. P. *J. Electroanal. Chem.* **1995**, *393*, 75.